Electrochimica Acta 444 (2023) 141974

Contents lists available at ScienceDirect

Electrochimica Acta

journal homepage: www.journals.elsevier.com/electrochimica-acta

Analysis of thermal and electrochemical properties of electrical double-layer capacitors by using an *in-situ* simultaneous thermal analysis cell

Annika Bothe [a], S.E.M. Pourhosseini [b], Paula Ratajczak [b], François Béguin [b], Andrea Balducci [a,*]

[a] *Institute for Technical Chemistry and Environmental Chemistry, Center for Energy and Environmental Chemistry Jena (CEEC Jena), Friedrich-Schiller-University Jena, Philosophenweg 7a, Jena 07743, Federal Republic of Germany*
[b] *Institute of Chemistry and Technical Electrochemistry, Poznan University of Technology, Berdychowo 4, Poznan 60-965, Poland*

ARTICLE INFO

Keywords:
In-situ STA
Thermal investigation
Heat flow
EDLC
Aging
Silica-templated carbon

ABSTRACT

In this work, the impact of temperature and voltage on aging of electrical double-layer capacitors (EDLCs) made with a model silica-templated carbon has been investigated by using an *in-situ* simultaneous thermal analysis (STA) cell. We show that the use of such a cell allows the electrochemical performance of EDLCs and the heat generation occurring within these devices to be simultaneously measured. In EDLCs containing adiponitrile (ADN) based electrolytes, the combination of high voltage ($\geq$ 3.5 V) and elevated temperature of 60 °C leads not only to a fast decrease in capacitance retention, but also to important degradation processes causing a significant increase of heat flow within the system. For a temperature of 60 °C, the heat flow at 3.75 V is about 6.5 times higher than in an EDLC operating at 3.0 V. The correlation of the heat flow and electrochemical properties provides a helpful insight into the stability of EDLCs, and thus the *in-situ* STA cell appears as an interesting and novel tool for the investigation of these systems.

1. Introduction

In order to minimize the possible fluctuations associated with the increasing use of renewable energy sources, the use of reliable and efficient energy storage systems (ESSs) is crucial [1]. Among the available ESSs, electrical double-layer capacitors (EDLCs) are nowadays considered as one of the most interesting. The dominating storage mechanism of EDLCs is based on the adsorption/desorption of ions onto/from the surface of electrodes, and the level of the redox reaction is negligible [2,3]. Therefore, they feature characteristics like high power density (up to 10 kW kg^{-1}), long cycle life ($>$ 1000,000) and a very short charge and discharge time (time frame of seconds, or less). On the other hand, due to their charge storage mechanism, the energy density of these devices is rather limited, especially when compared to that of lithium-ion batteries (LIBs) [4–7]. Due to these characteristics, EDLCs are particularly suitable for applications where a fast energy delivery and uptake is needed (e.g., gantry cranes, start-stop driving) as well as for stabilizing the power grid [8,9]. Commercial EDLCs consist of activated carbon (AC) electrodes combined with organic electrolytes containing acetonitrile (ACN) and an ammonium-based salt (in most of the cases tetraethyl ammonium tetrafluoroborate (Et_4NBF_4)) [10,11]. This electrode/electrolyte combination allows the realization of EDLCs operating up to 3.0 V [12]. In the last years, with the aim to increase the operating voltage, and thus the energy density of EDLCs, several alternative solvents (e.g., adiponitrile (ADN) [13,14], ethyl isopropyl sulfone (EiPS) [15,16]) and salts (e.g., 1,1-dimethyl pyrrolidinium tetrafluoroborate ($Pyr_{11}BF_4$) [17,18], 1-methyl-1-butyl pyrrolidinium tetrafluoroborate ($Pyr_{14}BF_4$) [19,20]) have been proposed [6]. None of these alternative components, however, has been so far implemented in large scale production.

In many applications, EDLCs experience a temperature which is not constant over time, e.g., by being exposed to the sun, by the presence of dissipating heat from surrounding components or by internal heat generation throughout cycling [21–23]. These changes, and especially those leading to temperatures higher than 60 °C, are strongly affecting the performance and the aging of EDLCs [22,24–28]. Therefore, a deep understanding of the temperature impact on the EDLCs behavior is of extreme importance for the development of these devices. Among the various approaches proposed to investigate the influence of temperature on the electrochemical performance of an EDLC, a convenient one is to

* Corresponding author.
E-mail address: andrea.balducci@uni-jena.de (A. Balducci).

https://doi.org/10.1016/j.electacta.2023.141974
Received 4 October 2022; Received in revised form 25 January 2023; Accepted 29 January 2023
Available online 31 January 2023

place it in a chamber at a defined temperature, e.g., 60 °C or 80 °C, and to monitor the electrochemical changes occurring within the cell [17,29,30]. If an accurate examination of the temperature evolution during cycling or floating is envisioned, the introduction of thermocouples outside of the device is a convenient and "easy to implement" strategy [23,31–33]. However, the utilization of thermocouples has the drawback of long residence times for the heat at boundaries. To overcome this limitation and gain more precise information about the thermal changes occurring in EDLCs, the use of an *in-operando* calorimeter has been proposed [34–36]. Through several studies, the group of Pilon showed that this approach allows the time-dependent heat generation to be investigated separately at each electrode during cycling [37–40]. Recently, with the aim to gain a deep understanding about these important processes, our group developed an *in-situ* simultaneous thermal analysis (STA) cell, which allows an accurate real time monitoring of heat flow and mass changes occurring in EDLCs while applying an electrochemical protocol. This *in-situ* STA cell is placed in a thermogravimetric analysis (TGA)/differential scanning calorimetry (DSC) device [41].

Using this innovative cell in the present study we analyzed the impact of the operating temperature and operating cell voltage on the heat flow variation occurring in EDLCs during float tests. The EDLCs incorporated electrodes made from a model silica-templated carbon (labeled STC-7), with negligible surface functionality, and the electrolyte was 1 M $Pyr_{14}BF_4$ in ADN.

2. Experimental

2.1. Porous carbon synthesis

The porous carbon used in this study has been prepared by adapting the method described in Ref. [42]. In brief, 53.3 g of a 30 wt.% suspension of colloidal silica in water (Ludox® SM, average particle size of 7 nm; W. R. GRACE) and 32 g of crystalline glucose were mixed in a beaker under stirring for 1 h. Then, the sample was transferred into a nickel crucible and dried in a stove at 70 °C for 48 h and was further pyrolyzed in a muffle furnace (FCF 2R, Czylok) at 900 °C for 2 h under nitrogen flow of 200 mL min^{-1}. After cooling to room temperature (RT), the thereof obtained carbon-silica composite (24.5 g) was leached twice in a 3 M NaOH (reagent grade; POCH) solution under reflux at 100 °C for 24 h to remove the silica template. Then, the solid residue (8.35 g) was washed several times with deionized water (5.5 μS cm^{-1}) until reaching a neutral pH of the filtrate. The sample was further dried in a stove at 120 ºC for 24 h and then ball-milled under air for 15 min at 400 rpm using a planetary ball mill (Pulverisette 7 premium line, Fritsch), tungsten carbide balls and jar (balls to carbon mass ratio of 15). Finally, the carbon was post-treated in a horizontal tubular furnace (PYROX) at 800 °C for 2 h under N_2 flow of 100 mL min^{-1} to eliminate the surface oxygenated functionalities; 8.0 g of porous carbons (carbonization yield of 25%) were obtained after this treatment. The prepared SiO_2-templated carbon will be further named "STC-7".

2.2. Porous carbon characterization

The oxygenated functionality of STC-7 was analyzed by temperature-programmed desorption (TPD) using a TG equipment (TG 209 F1 Iris, Netzsch) coupled with a mass spectrometer (QMS 403C Aeolos, Netzsch). The sample (~4 mg) was heated at 20 °C min^{-1} up to 950 °C under a helium flow (50 mL min^{1}). The CO_2 and CO evolving groups were quantified after calcium oxalate monohydrate calibration, considering CO disproportionation [43]. The mass loss reached 0.9 wt.% at 950 °C; the evolving gasses were CO_2 (0.11 mmol g^{-1}), CO (0.01 mmol g^{-1}), H_2O (0.12 mmol g^{-1}), with a total amount of evolved oxygen equal to 0.6 wt%. Such negligible values reveal a material with a very clean surface.

The porous texture of the STC-7 carbon was characterized by nitrogen adsorption/desorption at −196 °C using an ASAP 2020 (Micromeritics). Before the analyses, the sample was degassed at 350 °C under vacuum for 12 h. The pore size distribution (PSD) was determined by applying the two-dimensional non-local density functional theory (2D-NLDFT) and a dual shape pore model [44] with variable width limits interactively adjusted, w_s for the upper limit of the slit shape model and w_c for the lower limit of the cylindrical model [45]. The micro- and mesopore volumes (V_{micro} and V_{meso}) were estimated from the cumulative PSD. The micro- and mesopore sizes ($L_{0(micro)}$ and $L_{max(meso)}$) were taken as the average value for pores below 2 nm and at the maximum of PSD between 2 and 50 nm, respectively.

As it can be seen in Fig. 1a, STC-7 displays a type IV isotherm with an H1 hysteresis loop at high relative pressure ($P/P_0 > 0.6$) illustrating the multilayer adsorption in a narrow distribution of regular, well-defined cylindrical-like mesopores [46]. The pore size distribution (see Fig. 1b) shows that the material presents essentially mesopores with $L_{max(meso)} = 7.1$ nm, and a relatively negligible amount of micropores at $L_{0(micro)} = 0.55$ nm. The BET (S_{BET}) and cumulative surface areas (S_{DFT}) are 817 m^2 g^{-1} and 916 m^2 g^{-1}, respectively; the micro- and mesopore volumes are 0.09 cm^3 g^{-1} and 1.03 cm^3 g^{-1}.

The structure of the STC-7 carbon was investigated by Raman spectroscopy with a DXR-2 computer-controlled Raman spectroscope (ThermoFisher Scientific®) using a laser excitation wavelength of 532 nm and a small power of 2 mW with an exposure time of 30 s to avoid laser-induced heating of the samples. The spectra were deconvoluted using a Gaussian fitting function; the I_{D1}/I_{G1} intensity ratio was calculated using the fitted peak areas (so-called integrated intensities) [47].

The Raman spectrum of the STC-7 carbon (see Fig. 2) displays the characteristic *G* and *D* bands (centered at 1590 and 1334 cm^{-1}) arising from the sp^2 and sp^3/sp^2 hybridized carbon atoms, respectively [48]. The deconvolution of the spectrum reveals that the experimental signal consists of four peaks: (i) relatively narrow G_1 (at 1590 cm^{-1}) and D_1 bands (at 1351 cm^{-1}) attributed to the in-plane stretching (like E_{2g}) and breathing (like A_{1g}) vibration modes of the sp^2 pairs, respectively; and (ii) relatively broad G_2 (at 1537 cm^{-1}) and D_2 (at 1258 cm^{-1}) bands related to defect scattering; the G_2 band is associated with clusters of sp^2 hybridized amorphous carbons, whereas the D_2 band reflects the coexistence of sp^2 and sp^3 hybridized carbon atoms [49]. The I_{D1}/I_{G1} integrated intensity ratio of ~2 discloses that the STC-7 material consists of a relatively high proportion of amorphous-like carbon (short, distorted and disoriented layers) [50].

From the above presented TPD, nitrogen adsorption/desorption and Raman analyses, it can be then summarized that STC-7 is a very appropriate model material, with a clean surface and mesopores of very well controlled size, enabling to study the thermal and electrochemical properties of EDLCs implementing an organic electrolyte.

2.3. Electrolyte preparation

The solvent adiponitrile (ADN 99%, Sigma-Aldrich) was dried over molecular sieve until the water content was below 25 ppm (as measured by Karl-Fischer titration; C20, Mettler Toledo). The salt 1-butyl-1-methylpyrrolidinium tetrafluoroborate ($Pyr_{14}BF_4$, 99%, Iolitec) was dried in a glass oven (Büchi, B-585) at 80 °C under vacuum. The electrolyte 1 M $Pyr_{14}BF_4$ in ADN has been prepared in a glovebox under argon atmosphere (LabMaster Pro, MBraun, H_2O and $O_2 < 1$ ppm).

2.4. Electrodes preparation

Composite electrodes have been prepared utilizing the silica-templated STC-7 carbon as active material, Super C65 (Imerys Graphite & Carbon) as conductive additive and sodium carboxymethylcellulose (CMC, Walocell CRT 2000, DowWolff Cellulosics) as binder following a procedure similar to that explained in reference [51]. The ratio (in mass) between active material/conducting additive/binder in the dry electrodes was 90:5:5. The area of the electrodes utilized in the

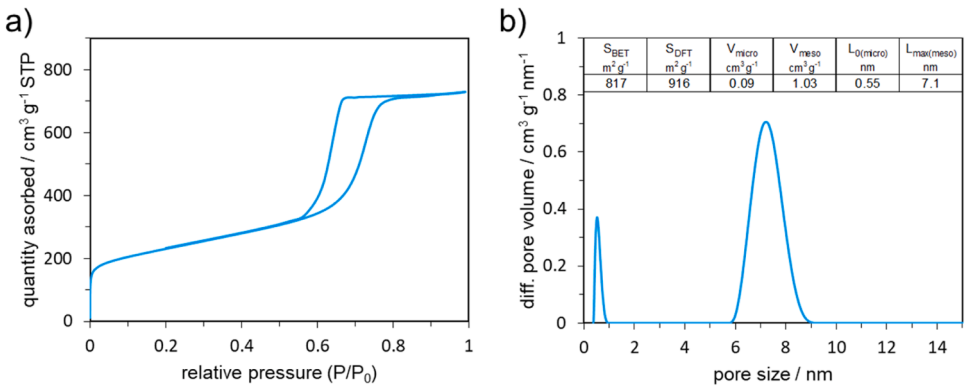

Fig. 1. (a) Nitrogen adsorption/desorption isotherm at −196 °C and (b) pore size distribution of the STC-7 carbon; the inset in Fig. 1 (b) shows the porous texture data.

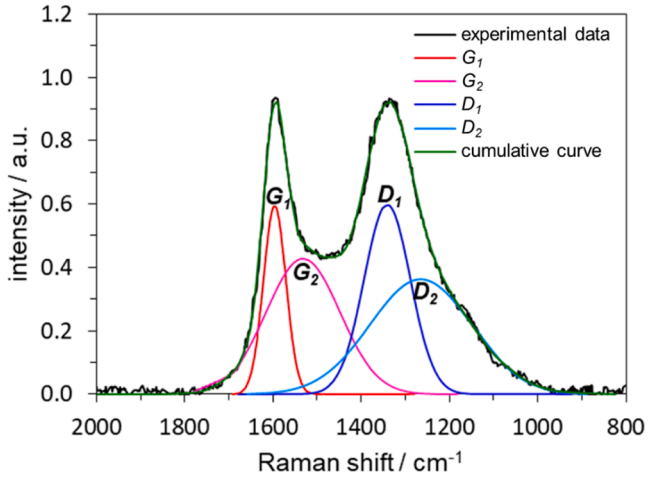

Fig. 2. Deconvoluted Raman spectrum of the STC-7 carbon with the fitted peaks attributed to the G_1, G_2, D_1 and D_2 bands. See the online article for the color version of this figure.

Swagelok cell set up (see below) was 1.13 cm^2 (∅ = 12 mm), whereas that of the electrodes utilized in the *in-situ* STA cell was 0.81 cm^2 (length: 1.8 mm and width: 0.45 mm). The active electrode mass loading (for Swagelok and *in-situ* STA electrodes) was ranging between 2 and 2.1 mg. The round electrodes were punched with a hollow punch, whereas the electrodes for the *in-situ* STA cell were hand cut with a scissor.

2.5. Electrochemical measurements

The electrochemical measurements have been carried out utilizing a Swagelok cell set up in a 2-electrode configuration or an *in-situ* STA cell, which were assembled in a glovebox (LabMaster Pro, MBraun, H_2O and $O_2 < 1$ ppm). A VMP3 multichannel potentiostat-galvanostat (BioLogic) and a LBT21084 multichannel potentiostatic–galvanostatic system (Arbin Instruments) were used for the Swagelok cells, whereas a SP150 (BioLogic) was used for the *in-situ* STA measurements.

In the Swagelok set up, EDLCs were assembled with two identical composite electrodes (2-electrode cell) separated by a Whatman GF/D glass microfiber filter (diameter: 13 mm, thickness: 670 μm) drenched with 120 μL of electrolyte. Initially, 50 charge-discharge cycles were carried out utilizing a current density of 1 A g^{-1}; subsequently, the stability of the EDLCs was evaluated by potentiostatic floating. During these tests, the cell was hold at either 3.0 V, 3.5 V or 3.75 V for 20 h and, afterwards, an impedance measurement was carried out (in a frequency range of 500 kHz to100 mHz). This procedure was repeated until a total float time of 100 h was reached. The tests have been realized at room temperature (RT) and 60 °C. At 60 °C, the floating time at constant voltage of 3.5 V and 3.75 V was reduced to 5 h.

The *in-situ* STA cell was assembled using two identical composite electrodes separated by a Whatman GF/A glass microfiber filter (length: 1.9 mm, width: 0.5 mm) drenched with 70 μL of electrolyte. Initially, the cell was left for 10 min at open circuit voltage (OCV). Afterwards, for conditioning, it was charged/discharge 5 times at a current density of 1 A g^{-1} from 0 V to the maximum operating voltage (either 3.0 V, 3.5 V or 3.75 V); every time the maximum voltage or 0 V were reached, they were kept at these values for 3 min. Subsequently, 20 charge-discharge cycles at 1 A g^{-1} were carried out between 0 V and the maximum operating voltage (either 3.0 V, 3.5 V or 3.75 V), followed by a constant voltage step for 5 h at the maximum operating voltage and an impedance measurement at the respective floating voltage. This procedure was repeated until a total float time of 40 h was reached. The measurements were performed at 30 °C and 60 °C. For the sake of completeness, all impedance spectra measured with the *in-situ* STA cell are shown in Fig. S1 of the supplementary information (SI).

2.6. In-situ STA measurements

All *in-situ* STA measurements were realized with a simultaneous TGA/DSC analyzer (PerkinElmer STA 6000). Before use, the system was purged with nitrogen (20 mL min^{-1}) for 1 h. For the performed measurements, the STA6000 was either held at 30 °C or 60 °C. To reach 60 °C, the temperature was increased at 10 °C min^{-1} starting from 30 °C.

3. Results and discussion

The *in-situ* STA cell considered in this work is shown in Fig. 3. The screws simplify the adjustment of the height and position of the cell inside the TGA/DSC device. This improvement compared to the one presented in our previous work [41] accelerates the procedure of setting up the measurement. As shown in Fig. 3a, the cell body consists of polyether ether ketone (PEEK) in which the EDLC is sandwiched between two titanium current collectors. Tiny screws at opposite sides are used to apply a pressure on the EDLC. Two enameled copper wires provide the connection between the cell and adjusting screws. A more detailed scheme of the cell can be found in Ref. [41].

The *in-situ* STA cell is an open system, which does not allow the use of volatile solvents like ACN. Therefore, as ADN is characterized by a low volatility, we decided to apply an ADN-based electrolyte which was recently investigated by our groups in Refs. [13,52], where the electrochemical stability limits and the degradation processes occurring in EDLCs containing this solvent were disclosed. Here, the aim of the study is to show the applicability of the *in-situ* STA cell for investigating the heat generation under high voltage operation of the EDLCs.

The average capacitance (with respect to the total active mass)

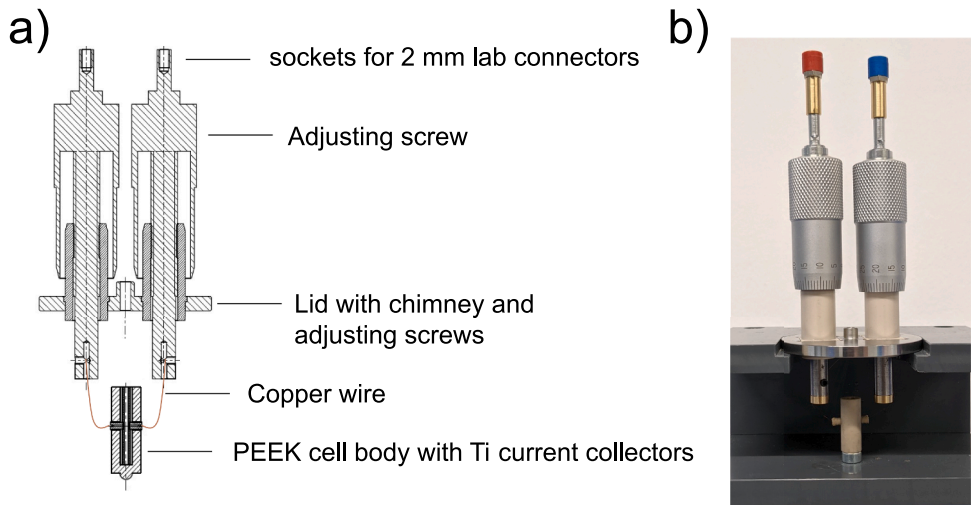

Fig. 3. *In-situ* STA cell, (a) scheme, (b) photography.

measured for the *in-situ* STA and Swagelok cells was of ca. 15 F g^{-1}. This value is lower than that reported for AC-based electrodes in the same electrolyte (*ca.* 20 F g^{-1}) [13]. Most probably, this difference is due to the relatively low specific surface area and relatively low amount of micropores of the silica-templated carbon used as an active material. Nonetheless, since the purpose of this study is to understand the impact of the EDLC stability while implementing a model carbon, the relatively low capacitance of the electrodes is not a problem. In fact, the negligible functionalization of the STC-7 material makes it very suitable for this investigation, where it is intended to mimic the phenomena occurring in industrial EDLCs implementing surface clean carbons. Considering the results of our previous study, three operating voltage (OPV) values have been considered for the *in-situ* STA cell, namely 3.0 V, 3.5 V and 3.75 V. The first value (3.0 V) has been selected as representative "stable OPV". The second value has been selected as "limit OPV", whereas the third one was chosen as "unstable OPV" [13,14].

Fig. 4 compares the stability of the EDLCs (using the *in-situ* STA cell) during float tests conducted at 30 °C and OPV values of 3.0 V, 3.5 V and 3.75 V. As shown in Fig. 4a, the capacitance decay of the devices increases with the OPV, reaching after 40 h of floating a capacitance retention of approx. 80%, 60% and 40% at OPVs of 3.0 V, 3.5 V and 3.75 V, respectively. The aging becomes visible in the Nyquist plots after 40 h of floating at 3.5 V and 3.75 V, which can be seen in a distortion caused by a very resistive behavior. On the other hand, the plot of the EDLC floated for 40 h at 3.0 V does not show any significant change in shape and only a slight increase in resistance compared to the Nyquist plot after 5 h of floating (see Fig. 4b and c). A full set of Nyquist plots recorded every 5 h of these experiments is presented in Fig. S1 of SI. Fig. S1 also reports the plots of specific capacitance (calculated from the EIS data) vs float time.

Fig. 5 compares the stability of the EDLCs during floating at 60 °C and OPV values of 3.0 V, 3.5 V and 3.75 V (using the *in-situ* STA cell). At this temperature, only the EDLC floated at 3.0 V exhibits a stable behavior, with a capacitance retention after 40 h comparable to that observed at 30 °C (see Fig. 4a). This is also well visible on the impedance spectra shown in Fig. 5b and c, where no significant increase in resistance can be seen (red line). For sake of comparison, the impedance spectra obtained for the EDLC after 40 h of floating at 3.0 V and 60 °C are reported in Fig. S2 of the supplementary information (SI). As shown in this figure, the impedance of this device increases slightly over the 40 h of floating time. On the other hand, the combination of high temperature and high voltage leads to a very fast performance fading, and the EDLCs floated at 3.5 V and 3.75 V do not display any capacitance after 20 and 10 h of floating, respectively (Fig. 5a). The impedance spectrum of the EDLC floated at 3.75 V underlines already very resistive characteristics after 5 h of floating (see Fig. 5b). After 20 h of floating (Fig. 5c), only the EDLC floated at 3.0 V exhibits a moderate resistance, as compared to the one floated at 3.75 V.

In our previous work, we observed that the stability is higher during a float test in a closed system (Swagelok cell) than in an opened system (*in-situ* STA cell), where the solvent of the electrolyte might evaporate [41]. For this reason, we have also performed measurements with

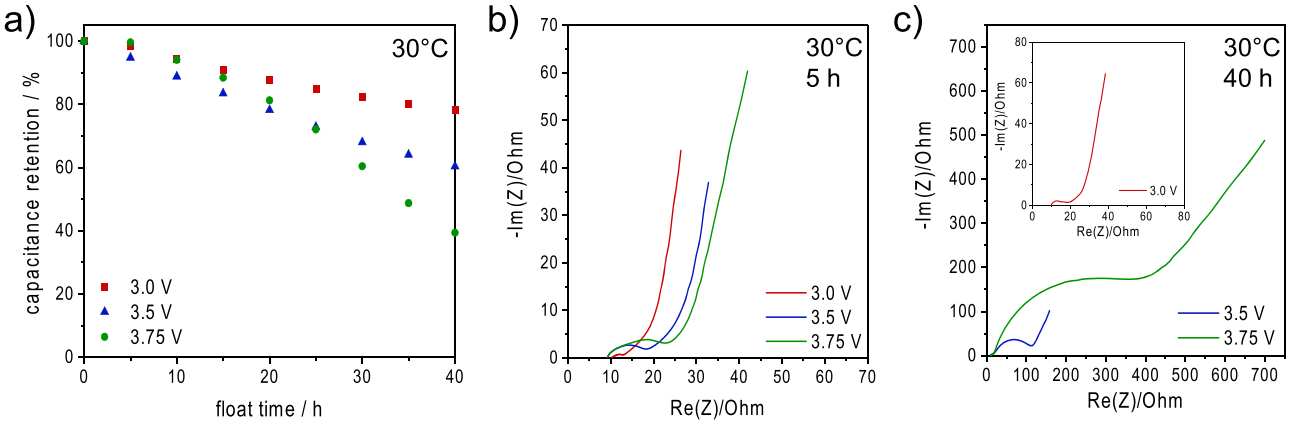

Fig. 4. Effect of floating performed with the *in-situ* STA cell at 30 °C on: (a) the capacitance retention, (b) the Nyquist plots after 5 h of floating (c) the Nyquist plots after 40 h of floating.

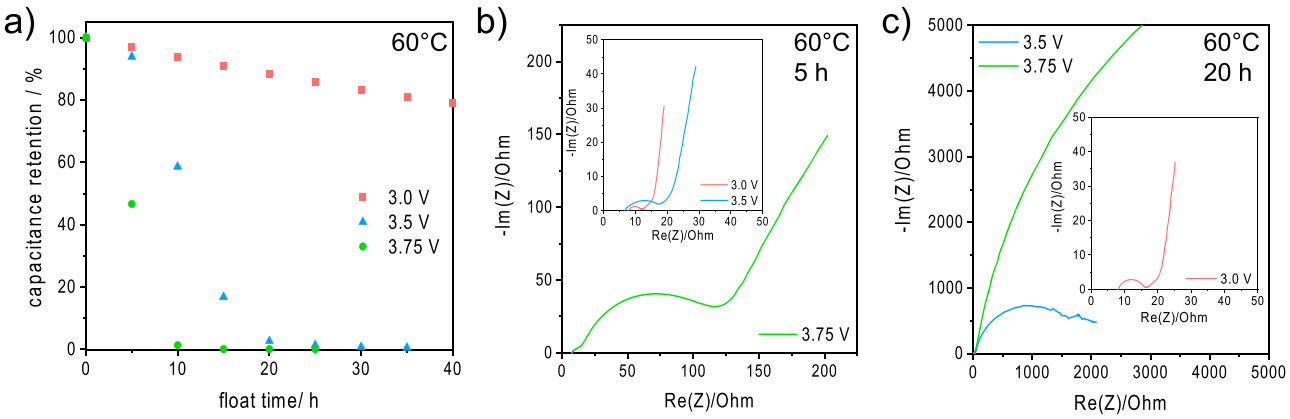

Fig. 5. Effect of floating performed with the *in-situ* STA cell at 60 °C on: (a) the capacitance retention, (b) the Nyquist plots after 5 h of floating, (c) the Nyquist plots after 20 h of floating.

Swagelok cells to verify if the results obtained with the *in-situ* STA cell are comparable with those obtained in "conventional" lab-scale devices. As shown in Figs. S3–S5 of the SI, the use of the two cells indeed leads to comparable results. Thus, the outcomes from the experiments realized with the *in-situ* STA cell can be considered as representative of the systems containing the investigated electrode-electrolyte combination.

Fig. 6 compares the cumulative heat flow recorded during the float test discussed in the previous figures (Figs. 4 and 5). For this purpose, the cumulative heat flow was corrected by subtracting the baseline determined when the STA measurement was realized without applying any electrochemical protocol (Fig. S6 of the SI). As it can be seen in Fig. 6a, the cumulative heat flow over the floating time at 30 °C increases in subsequent steps (appearing in the figure as a staircase). This peculiar shape derived from the electrochemical protocol applied to the cell, and each step corresponds to the floating period at a constant voltage. As shown, the higher the OPV, the higher the total heat flow, indicating that the amount of ions adsorbing/desorbing onto/from the electrodes surface increases with the OPV [38]. Additionally, it is visible that at OPV of 3.5 V and 3.75 V the distance between the steps increases with the floating time. Compared to the first step, the rise for the 8th step is ca. 67% and 39% higher when floating the EDLC at 3.75 V and 3.5 V, respectively. This increase indicates that some additional heat is generated due to progressive decomposition reactions of the electrolyte, which is in accordance with Fig. 4a showing a diminishing capacitance retention. During floating at 3.0 V, however, the magnitude of the steps stays more or less constant over the time of the experiment.

Interestingly, when increasing the floating temperature to 60 °C (Fig. 6b), the "staircase pattern" previously observed at 30 °C was only obtained for the device operating at 3.0 V. At higher OPVs, the steps are only visible within the first 10 to 20 h. In the case of the EDLC operating at 3.5 V the magnitude of the first step is rather comparable to that observed at the same OPV at 30 °C. Afterwards, a large increase in heat flow for each step is monitored, and after 20 h of floating an irregular heat generation is detected, implying an increase in resistance and electrolyte decomposition. In the case of the EDLC floated at 3.75 V, the magnitude of the first two steps is significantly larger than at 30 °C. This higher heat flow indicates that directly from the beginning of the measurement, additional heat is generated, e.g., due to electrolyte decomposition and an increase in resistance. After this initial increase, no change in heat flow was detected, showing that the EDLC is not working any longer and no electric double-layer can be formed. These findings are in very good agreement with the electrochemical performance discussed in the previous section (see Fig. 5). For a better comparison of the heat flow measured at 30 °C and 60 °C, the slope of the cumulative heat flow between 0 and 10 h was fitted linearly and is compared in Fig. 6c. The time was limited to 10 h to allow the EDLC floated at 3.75 V and 60 °C to be included in the comparison of the various measurements. As shown in Fig. 6c, an increase of OPV leads to an increase of the heat flow within the EDLCs, and the growth is more significant at 60 °C than 30 °C. In the case of the cells floated at 3.0 V (red columns), the heat flow slightly decreases with increasing temperature. This behavior can be explained by considering the decrease of viscosity and better transport properties of the electrolyte at higher temperature, resulting in a lower resistance of the device and finally leads to a lower heat generation (in this first 10 h). This is supported by taking a closer look at the impedance spectra after 5 h and 10 h of floating at 3.0 V at 30 °C and 60 °C (see Fig. S7 of SI). The Nyquist plots of the measurements performed at 60 °C display a lower resistance compared to the measurements at 30 °C. The slope of the cumulative heat flow measured at 60 °C for a floating voltage of 3.75 V and 3.5 V is about 6.5 and 3.5 times higher, respectively, than at 3.0 V. However, at 30 °C, the respective ratios of only about 2 (3.75 V) and 1.4 (3.5 V), indicate much lower heat generation than at 60 °C.

Hence, the above reported results demonstrate that the *in-situ* STA cell enables to simultaneously measure the electrochemical performance of EDLCs and the heat generation occurring within these devices. The correlation of these two fundamental parameters gives an additional insight into understanding the impact of the operating conditions on the EDLCs performance.

4. Conclusion

In this study, we reported the use of an innovative *in-situ* STA cell for investigating the impact of operating temperature and operating voltage on the performance of EDLCs. We showed that the use of this cell allows a simultaneous measurement of the electrochemical performance of EDLCs (in a manner comparable to that of conventional lab-scale cells) and of the heat generated within these devices. The correlation of these two key parameters provides a very helpful insight about the stability of EDLCs. We demonstrated that when ADN-based EDLCs work at 60 °C and a voltage of 3.5 V (or higher), an important degradation process occurs. This deterioration leads to about 6.5 times (under floating at 3.75 V) and 3.5 times (under floating at 3.5 V) higher internal heat flow as compared to that occurring in the EDLC floated at 3 V. In contrast, when the same voltage conditions are applied at 30 °C, the increase in heat flow is only a fraction of the values found at 60 °C.

Taking these results into account, the *in-situ* STA cell appears as an interesting and novel tool for the investigation of EDLCs. In the future, the use of the cell can be extended for the investigation of other alternative electrolytes e.g., ionic liquids. Furthermore, the connection of the cell with a TGA/DSC and with a FT/IR-GC/MS can give the possibility to correlate the formation of any decomposition products to the state-of-health of the EDLC.

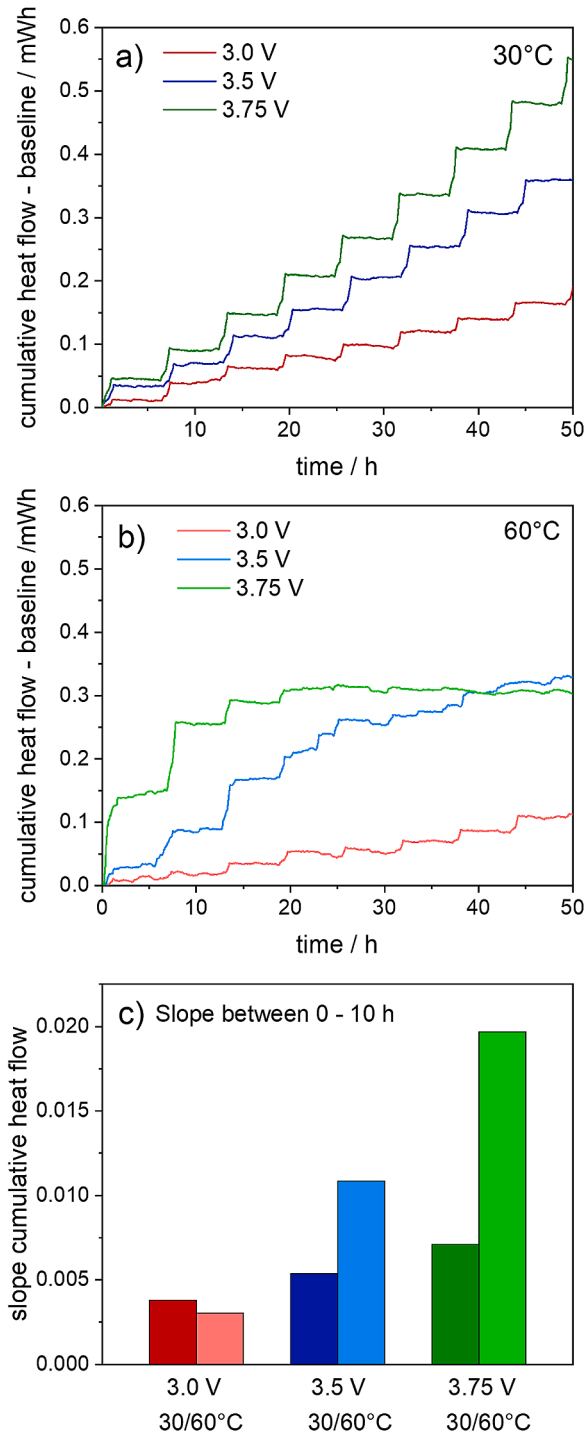

Fig. 6. Cumulative heat flow after baseline correction (a) 30 °C, (b) 60 °C and (c) slope of the cumulative heat flow after baseline correction (taken between 0 and 10 h) for 30 °C and 60 °C.

CRediT authorship contribution statement

Annika Bothe: Writing – original draft, Investigation, Formal analysis. **S.E.M. Pourhosseini:** Investigation, Formal analysis. **Paula Ratajczak:** Writing – original draft. **François Béguin:** Writing – original draft, Supervision. **Andrea Balducci:** Writing – original draft, Supervision.

Declaration of Competing Interest

The authors declare no conflict of interest.

Data availability

Data will be made available on request.

Acknowledgments

A.B. and A.B. wish to thank the Deutsche Forschungsgemeinschaft (DFG) [project BA4956/8-1] for the financial support. The authors would also like to acknowledge F.B., S.E.M.P. and P.R. wish to thank the Polish National Science Center (NCN) [Beethoven project UMO-2016/23/G/ST4/04186] for the financial support. The authors would also like to acknowledge Dr. Agnieszka Chojnacka for Raman analysis and processing gas adsorption data; they are also grateful to W. R. GRACE for kindly providing the Ludox® colloidal silica.

Supplementary materials

Supplementary material associated with this article can be found, in the online version, at doi:10.1016/j.electacta.2023.141974.

References

[1] A. Kalair, N. Abas, M.S. Saleem, A.R. Kalair, N. Khan, Role of energy storage systems in energy transition from fossil fuels to renewables, Energy Storage 3 (1) (2021) e135.
[2] J. Zhao, A.F. Burke, Review on supercapacitors: technologies and performance evaluation, J. Energy Chem. 59 (2021) 276–291.
[3] A.C. Forse, C. Merlet, J.M. Griffin, C.P. Grey, New perspectives on the charging mechanisms of supercapacitors, J. Am. Chem. Soc. 138 (18) (2016) 5731–5744.
[4] B. Babu, P. Simon, A. Balducci, Fast charging materials for high power applications, Adv. Energy Mater. 10 (29) (2020), 2001128.
[5] P. Simon, Y. Gogotsi, Materials for electrochemical capacitors, Nat. Mater. 7 (11) (2008) 845–854.
[6] P. Simon, Y. Gogotsi, Perspectives for electrochemical capacitors and related devices, Nat. Mater. 19 (11) (2020) 1151–1163.
[7] F. Béguin, V. Presser, A. Balducci, E. Frackowiak, Carbons and electrolytes for advanced supercapacitors, Adv. Mater. 26 (14) (2014) 2219–2251.
[8] C. Schütter, S. Pohlmann, A. Balducci, Industrial requirements of materials for electrical double layer capacitors: impact on current and future applications, Adv. Energy Mater. 9 (25) (2019), 1900334.
[9] J.R. Miller, A.F. Burke, Electrochemical capacitors: challenges and opportunities for real-world applications, Electrochem. Soc. Interface 17 (1) (2008) 53.
[10] A. Balducci, Electrolytes for high voltage electrochemical double layer capacitors: a perspective article, J. Power Sources 326 (2016) 534–540.
[11] C. Zhong, Y. Deng, W. Hu, J. Qiao, L. Zhang, J. Zhang, A review of electrolyte materials and compositions for electrochemical supercapacitors, Chem. Soc. Rev. 44 (21) (2015) 7484–7539.
[12] P. Kurzweil, J. Schottenbauer, C. Schell, Past, present and future of electrochemical capacitors: pseudocapacitance, aging mechanisms and service life estimation, J. Energy Storage 35 (2021), 102311.
[13] A. Bothe, S.E.M. Pourhosseini, P. Ratajczak, F. Beguin, A. Balducci, Towards understanding the impact of operating voltage on the stability of adiponitrile-based electrical double-layer capacitors, J. Power Sources 496 (2021), 229841.
[14] A. Brandt, P. Isken, A. Lex-Balducci, A. Balducci, Adiponitrile-based electrochemical double layer capacitor, J. Power Sources 204 (2012) 213–219.
[15] K. Chiba, T. Ueda, Y. Yamaguchi, Y. Oki, F. Shimodate, K. Naoi, Electrolyte systems for high withstand voltage and durability I. linear sulfones for electric double-layer capacitors, J. Electrochem. Soc. 158 (8) (2011) A872.
[16] C. Schütter, A. Bothe, A. Balducci, Mixtures of acetonitrile and ethyl isopropyl sulfone as electrolytes for electrochemical double layer capacitors, Electrochim. Acta 331 (2020), 135421.
[17] L. Köps, F.A. Kreth, A. Bothe, A. Balducci, High voltage electrochemical capacitors operating at elevated temperature based on 1,1-dimethylpyrrolidinium tetrafluoroborate, Energy Storage Mater. 44 (2022) 66–72.
[18] H.V.T. Nguyen, K. Kwak, K.K. Lee, 1,1-Dimethylpyrrolidinium tetrafluoroborate as novel salt for high-voltage electric double-layer capacitors, Electrochim. Acta 299 (2019) 98–106.
[19] J. Krummacher, C. Schütter, S. Passerini, A. Balducci, Characterization of different conductive salts in ACN-based electrolytes for electrochemical double-layer capacitors, ChemElectroChem 4 (2) (2017) 353–361.
[20] S. Pohlmann, R.S. Kühnel, T.A. Centeno, A. Balducci, The influence of anion–cation combinations on the physicochemical properties of advanced electrolytes for

supercapacitors and the capacitance of activated carbons, ChemElectroChem 1 (8) (2014) 1301–1311.
[21] M. Haque, Q. Li, A.D. Smith, V. Kuzmenko, E. Köhler, P. Lundgren, P. Enoksson, Thermal influence on the electrochemical behavior of a supercapacitor containing an ionic liquid electrolyte, Electrochim. Acta 263 (2018) 249–260.
[22] H. Gualous, D. Bouquain, A. Berthon, J.M. Kauffmann, Experimental study of supercapacitor serial resistance and capacitance variations with temperature, J. Power Sources 123 (1) (2003) 86–93.
[23] M. Al Sakka, H. Gualous, J. Van Mierlo, H. Culcu, Thermal modeling and heat management of supercapacitor modules for vehicle applications, J. Power Sources 194 (2) (2009) 581–587.
[24] M. Hahn, R. Kötz, R. Gallay, A. Siggel, Pressure evolution in propylene carbonate based electrochemical double layer capacitors, Electrochim. Acta 52 (4) (2006) 1709–1712.
[25] S.I. Fletcher, F.B. Sillars, R.C. Carter, A.J. Cruden, M. Mirzaeian, N.E. Hudson, J. A. Parkinson, P.J. Hall, The effects of temperature on the performance of electrochemical double layer capacitors, J. Power Sources 195 (21) (2010) 7484–7488.
[26] R. Kötz, M. Hahn, R. Gallay, Temperature behavior and impedance fundamentals of supercapacitors, J. Power Sources 154 (2) (2006) 550–555.
[27] O. Bohlen, J. Kowal, D.U. Sauer, Ageing behaviour of electrochemical double layer capacitors: part I. Experimental study and ageing model, J. Power Sources 172 (1) (2007) 468–475.
[28] P. Kurzweil, A. Hildebrand, M. Weiß, Accelerated life testing of double-layer capacitors: reliability and safety under excess voltage and temperature, ChemElectroChem 2 (1) (2015) 150–159.
[29] X. Li, W. Li, Q. Liu, S. Chen, L. Wang, F. Gao, G. Shao, Y. Tian, Z. Lin, W. Yang, Robust high-temperature supercapacitors based on SiC nanowires, Adv. Funct. Mater. 31 (8) (2021), 2008901.
[30] M. Lazzari, F. Soavi, M. Mastragostino, Mesoporous carbon design for ionic liquid-based, double-layer supercapacitors, Fuel Cells 10 (5) (2010) 840–847.
[31] H. Gualous, H. Louahlia, R. Gallay, Supercapacitor characterization and thermal modelling with reversible and irreversible heat effect, IEEE Trans. Power Electron. 26 (11) (2011) 3402–3409.
[32] J. Schiffer, D. Linzen, D.U. Sauer, Heat generation in double layer capacitors, J. Power Sources 160 (1) (2006) 765–772.
[33] H. Gualous, H. Louahlia-Gualous, R. Gallay, A. Miraoui, Supercapacitor thermal modeling and characterization in transient state for industrial applications, IEEE Trans. Ind. Appl. 45 (3) (2009) 1035–1044.
[34] C. Pascot, Y. Dandeville, Y. Scudeller, P. Guillemet, T. Brousse, Calorimetric measurement of the heat generated by a double-layer capacitor cell under cycling, Thermochim. Acta 510 (1) (2010) 53–60.
[35] P. Guillemet, C. Pascot, Y. Scudeller, Electro-thermal analysis of electric double-layer-capacitors, in: Proceedings of the 2008 14th International Workshop on Thermal Inveatigation of ICs and Systems, 2008.
[36] Y. Dandeville, P. Guillemet, Y. Scudeller, O. Crosnier, L. Athouel, T. Brousse, Measuring time-dependent heat profiles of aqueous electrochemical capacitors under cycling, Thermochim. Acta 526 (1) (2011) 1–8.
[37] O. Munteshari, J. Lau, A. Krishnan, B. Dunn, L. Pilon, Isothermal calorimeter for measurements of time-dependent heat generation rate in individual supercapacitor electrodes, J. Power Sources 374 (2018) 257–268.
[38] O. Munteshari, A. Borenstein, R.H. DeBlock, J. Lau, G. Whang, Y. Zhou, A. Likitchatchawankun, R.B. Kaner, B. Dunn, L. Pilon, In operando calorimetric measurements for activated carbon electrodes in ionic liquid electrolytes under large potential windows, ChemSusChem 13 (5) (2020) 1013–1026.
[39] A. Likitchatchawankun, G. Whang, J. Lau, O. Munteshari, B. Dunn, L. Pilon, Effect of temperature on irreversible and reversible heat generation rates in ionic liquid-based electric double layer capacitors, Electrochim. Acta 338 (2020), 135802.
[40] A. Likitchatchawankun, R.H. DeBlock, G. Whang, O. Munteshari, M. Frajnkovič, B. S. Dunn, L. Pilon, Heat generation in electric double layer capacitors with neat and diluted ionic liquid electrolytes under large potential window between 5 and 80°C, J. Power Sources 488 (2021), 229368.
[41] L.H. Hess, A. Bothe, A. Balducci, Design and use of a novel *in situ* simultaneous thermal analysis cell for an accurate "real time" monitoring of the heat and weight changes occurring in electrochemical capacitors, Energy Technol. 9 (9) (2021), 2100329.
[42] N. Bhandari, R. Dua, L. Estevez, R. Sahore, E.P. Giannelis, A combined salt–hard templating approach for synthesis of multi-modal porous carbons used for probing the simultaneous effects of porosity and electrode engineering on EDLC performance, Carbon N. Y. 87 (2015) 29–43.
[43] J. Wang, B. McEnaney, Quantitative calibration of a TPD-MS system for CO and CO_2 using calcium carbonate and calcium oxalate, Thermochim. Acta 190 (2) (1991) 143–153.
[44] J. Jagiello, A. Chojnacka, S.E.M. Pourhosseini, Z. Wang, F. Beguin, A dual shape pore model to analyze the gas adsorption data of hierarchical micro-mesoporous carbons, Carbon N. Y. 178 (2021) 113–124.
[45] J. Jagiello, J. Castro-Gutiérrez, R.L.S. Canevesi, A. Celzard, V. Fierro, Comprehensive analysis of hierarchical porous carbons using a dual-shape 2D-NLDFT model with an adjustable slit–cylinder pore shape boundary, ACS Appl. Mater. Interfaces 13 (41) (2021) 49472–49481.
[46] M. Thommes, K. Kaneko, A.V. Neimark, J.P. Olivier, F. Rodriguez-Reinoso, J. Rouquerol, K.S.W. Sing, Physisorption of gases, with special reference to the evaluation of surface area and pore size distribution (IUPAC Technical Report), Pure Appl. Chem. 87 (9–10) (2015) 1051–1069.
[47] A.C. Ferrari, J. Robertson, Interpretation of Raman spectra of disordered and amorphous carbon, Phys. Rev. B 61 (20) (2000) 14095–14107.
[48] K.W.R. Gilkes, H.S. Sands, D.N. Batchelder, W.I. Milne, J. Robertson, Direct observation of sp3 bonding in tetrahedral amorphous carbon UV Raman spectroscopy, J. Non Cryst. Solids 227–230 (1998) 612–616.
[49] A. Coccato, J. Jehlicka, L. Moens, P. Vandenabeele, Raman spectroscopy for the investigation of carbon-based black pigments, J. Raman Spectrosc. 46 (10) (2015) 1003–1015.
[50] M. Pawlyta, J.N. Rouzaud, S. Duber, Raman microspectroscopy characterization of carbon blacks: spectral analysis and structural information, Carbon N. Y. 84 (2015) 479–490.
[51] A. Krause, P. Kossyrev, M. Oljaca, S. Passerini, M. Winter, A. Balducci, Electrochemical double layer capacitor and lithium-ion capacitor based on carbon black, J. Power Sources 196 (20) (2011) 8836–8842.
[52] S.E.M. Pourhosseini, A. Bothe, A. Balducci, F. Beguin, P. Ratajczak, Strategy to assess the carbon electrode modifications associated with the high voltage ageing of electrochemical capacitors in organic electrolyte, Energy Storage Mater. 38 (2021) 17–29.